Nuclear magnetic resonance studies of xenon clusters in zeolite Na*A*

Cynthia J. Jameson
Department of Chemistry M/C-111, University of Illinois at Chicago, Chicago, Illinois 60680

A. Keith Jameson
Department of Chemistry, Loyola University, Chicago, Illinois 60626

Rex Gerald II and Angel C. de Dios
Department of Chemistry M/C-111, University of Illinois at Chicago, Chicago, Illinois 60680

(Received 5 September 1991; accepted 18 October 1991)

We have observed the equilibrium distribution of Xe atoms trapped in the alpha cages of zeolite Na*A* at 300 and at 360 K for low to high xenon loadings. The experimental distributions obtained by nuclear magnetic resonance (NMR) spectroscopy differ from two previously proposed statistical distributions. The experimental deviations from these statistical models can be explained by the attractive Xe–Xe interactions which favor clustering at low to medium loading, and the higher energies associated with the overcrowded cage disfavoring clusters of eight Xe atoms at high loadings. The temperature dependence of the ^{129}Xe NMR chemical shift of each cluster has been measured in the range 188–421 K, except that for Xe_8, which was determined only up to 300 K. The observed shifts and their temperature dependence are interpreted by using the results of *ab initio* calculations of the intermolecular shielding function in the ^{39}Ar system as a model for the ^{129}Xe system.

I. INTRODUCTION

Zeolites provide a continuous network of absolutely regular small diameter pores of molecular size. This forms the basis for the use of these molecular sieves in separation of gases and liquids and in catalysis. Of considerable current interest are practical methods of characterization of the inner surfaces which, if properly understood, may be able to reveal details of the internal structure of other microporous solids and lead to an understanding of the mechanisms by which the inner structure of these crystalline materials act as solid enzymes.[1]

At the same time, studies of the guest molecules inside zeolites are interesting in their own right. The microporous zeolite frameworks provide the perfect regularity needed for study of the fundamental events in sorption and catalysis under ambient rather than ultrahigh vacuum conditions. When the pore width is of the order of molecular dimensions, then the molecules can behave as a quasi-two-dimensional fluid.[2] When the size of the guest molecule and the entrances to the internal cavities are comparable, confinement of the guest molecules can occur. The problems of understanding how the structure and transport of fluids are altered by geometric confinement are of recent theoretical interest (see, e.g., Refs. 2–5). One of the most demanding tests of theories of strongly inhomogeneous fluids is the prediction of the density distribution of a fluid between solid surfaces. The theory must account successfully for the finite size of the particles which give rise to the excluded volume effects that partly determine the equilibrium density distribution. Especially interesting are fluids in pores less than four molecular diameters wide. Many properties of fluids in porous media become inaccessible to experimental measurement when the pore size approaches molecular dimensions. Thus, molecular dynamics simulations commonly take the role of experiment in testing approximate theoretical models. Some of the "observables" used in these comparisons are (a) the particle distribution function; (b) the self-diffusion coefficients; (c) adsorption isotherms. When the pore width becomes small enough, the effective dimensionality of the fluid is reduced. For planar solid walls, calculations have shown that a pore width of less than 2.5 molecular diameters is sufficient to keep the fluid in the quasi-two-dimensional regime.[2]

Magnetic resonance is particularly useful to obtain information on two-dimensional systems. The theory of spin relaxation rates T_1^{-1} and T_2^{-1} by translational diffusion in two-dimensional planar or spherical systems has been derived[6,7] and the logarithmic frequency dependence of T_1^{-1} has been verified experimentally by the recent studies of Jonas *et al.*[8] The nuclear magnetic resonance (NMR) pulsed field gradient technique has been used to study the intracrystallite diffusion of xenon adsorbed in zeolites.[9] Molecular dynamics simulations and Monte Carlo techniques applied to the motion of methane molecules within zeolites have been reported by several laboratories.[10–14] These simulations can produce self-diffusivities, heats of adsorption, and adsorption isotherms in zeolite systems. Molecular dynamics calculations by Theodorou and co-workers[13] have resulted in single particle density distribution functions, adsorption isotherms, and self-diffusivity of xenon in silicalite (like zeolite ZSM-5, but contains no Al atoms) at various xenon loadings at temperatures of 200, 300, and 400 K. The self-diffusivities measured by Pfeifer and co-workers[9] are in good agreement with the calculations for loadings ranging from 4–12 Xe atoms/unit cell.

One of the methods of characterizing zeolites is by means of ^{129}Xe NMR spectroscopy. The very large chemical

 0021-9606/92/031676-14$06.00

shifts of this nucleus and its sensitivity to intermolecular interactions was first established in the gas phase,[15-17] and Xe has since been used as a van der Waals probe in liquid crystals[18-20] and solutions,[21,22] even in biological systems. The introduction of Xe NMR spectroscopy into characterization of zeolites by Fraissard and Ito has resulted in a large number of studies in which the Xe chemical shift has been found to vary with zeolite pore and channel dimensions, with the distribution of cations and coadsorbed molecules, with dispersed metal atoms, and with water content.[23,24] The major breakthroughs have been in the application of Xe NMR spectroscopy to the estimation of pore sizes in various materials.[25-28] Xe chemical shifts in the presence of other guest molecules have been used to study the distribution of guest molecules in the zeolites.[29] Although many interesting and useful trends have been established, what is still missing from these studies is a basic understanding of the relationship of the average chemical shift to cavity size, to average xenon loading, temperature, presence, and type of counterions or guests. These questions are all related to intermolecular effects on the NMR chemical shift, which we have studied previously in the gas phase.

In these two papers, we report the results of systematic, controlled experiments for a given zeolite of known structure. We carry out variable temperature studies at 188–420 K and variable xenon loading over a wider range than ever done before. Our ability to operate at elevated pressures allows us to make measurements at high xenon loading at temperatures much higher than the 144 K of previous work,[30] such that we can observe systems which are at equilibrium. The limited mobility of Xe in zeolite at low temperatures precludes equilibration in finite times.

For our studies, we choose the zeolite *A* which provides perhaps the simplest environment for xenon. The framework Si/Al ratio in zeolite *A* is 1.0; the structure is simple enough for all ions to be locatable.[31] There are 12 Na^+ ions per pseudounit cell. Entry into each large cavity (called an alpha cage) can be made from six others arranged octahedrally through the six eight-ring (i.e., eight oxygens arranged in a plane) windows. There are smaller cavities (called beta cages) in the sodalite units, which can be entered only through a six-ring window which is far too small to be entered by Xe atoms. The low-dimensional systems studied here are small xenon clusters in zeolite Na*A*, where every window of each alpha cage, in which the xenons can be trapped, is partly blocked by Na^+ ions. We obtain the xenon atom distributions associated with various xenon loadings, i.e., we are able to determine P_n, the fraction of the alpha cages containing n Xe atoms. These distributions give a measure of the fluctuations in the number of particles. We compare these experimental distributions with two models for the strictly statistical distribution of hard spheres in subvolumes. In the future, we hope to be able to do molecular dynamic simulations using realistic potentials including, e.g., the best characterization of the Xe–Xe interaction to be constructed to date.[32] Currently, there are Monte Carlo[33,34] and molecular dynamics simulations of Xe atoms in zeolites *X* and *Y*,[35,36] and in silicalite[13] using potential functions which are based largely on the work of Kiselev and Du.[37]

In the paper which follows this one, we study Xe atoms inside zeolite Ca*A* which has the same framework structure, but with known differences in the locations of counterions compared to Na*A*.[38]

II. EXPERIMENT

We prepare approximately 50 mg of zeolite in a small sample tube and introduce xenon such that the final pressure can be as high as 50 atm. Our method suffers from having a low "filling factor" such that long acquisition times are commonly needed. Its advantages are that the contained zeolite mass, xenon mass, and tube volume are known quantitatively and do not change with time. Furthermore, we are able to produce xenon loadings in which the zeolite cage is completely filled with the molecules under study, xenon in this instance. This method allows variable temperature studies of truly equilibrium samples at loadings all the way up to completely full alpha cages.

Samples are prepared using ordinary (undersized) 4 mm o.d. borosilicate tubing which will just fit inside 5 mm diameter NMR tubes. The inside diameter is about 2.2 mm and the final tube length is 5 cm. This is a convenient length which can be entirely dewared in the probe, an absolute necessity for precise work. Typical volumes are 0.2–0.25 cm^3. These sample tubes are annealed overnight. Previously dried zeolite and a small plug of glass wool are then introduced. A ground glass joint and a Young cylindrically symmetric stopcock is attached, creating an assembly which can be moved without breaking a vacuum, but which has only 2–3 ml of "dead volume."

At this point, final dehydration is accomplished in order to remove any trace of water which may have been adsorbed during introduction of the typically 40–60 mg of zeolite into the sample tube. The zeolite is dehydrated for 10–16 h at 350 °C under thin bed conditions ($\sim$1 mm bed thickness) under vacuum.

After dehydrating the zeolite, the sample tubes can be moved to the standard vacuum line which we use to introduce a known quantity of xenon into the zeolite samples. The xenon is degassed by several freeze–thaw cycles under liquid nitrogen on the vacuum line. Expansion at a measured low pressure into a calibrated volume at room temperature provides a known number of moles of xenon. All the gas in the calibrated volume is swept out with mercury for a quantitative transfer into the sample tube. The tube is then sealed off under liquid nitrogen and heated in an oven at 450 K for 30 min or longer, a temperature significantly higher than the highest temperature (420 K) which the NMR probe will attain. Our experience is that errors in the preparation of the samples are equivalent to an approximately 2% relative error in the gas density within the tube.

Equilibration of the samples at 300 K is extremely slow since the xenon atoms must diffuse slowly to the empty centers of the crystallites. To accelerate the approach to equilibrium, we place the samples in an oven at 500 K for 2 h and reduce the temperature in a programmed manner over several days. The high temperature distributions are reached

rapidly and then the final 300 K equilibration involves relatively minor changes in mass transport. In this manner, equilibrium at 300 K can be attained in under two months.

In samples prepared as described, a mass balance calculation yields the xenon contained inside the zeolite as the xenon initially frozen into the tube minus the xenon still in the gas external to the zeolite crystallites. The number of moles in the gas phase is determined from the density of the free gas, known from the measured resonance frequency of the gas peak

$$\sigma(\rho,T) = \sigma_0 + \sigma_1(T)\rho + \sigma_2(T)\rho^2 + \cdots, \quad (1)$$

which we determined some time ago.[16] Here, ρ is the gas density in amagats (1 amagat is the number density equal to 2.687×10^{19} molecules/cm^3). At densities below about 100 amagats $\sigma_2(T)\rho^2$ can be ignored and $\sigma_1(T)$ is obtained from our previous work,[16] including the bulk susceptibility term for a cylindrical sample parallel to the magnetic field. σ_0 is the shielding of the isolated xenon atom. Therefore, measuring the resonance frequency allows calculation of the gas density. From the known free volume, the number of moles of xenon remaining outside the zeolite can be determined. We determine the number of xenon atoms inside the zeolite by difference and hence know the average number of xenon atoms per alpha cage $\langle n\rangle$ for any measured resonance frequency of the gas peak in a sample at any temperature.

NMR measurements were carried out on a Bruker AM400 spectrometer. The temperature was monitored using ethylene glycol (above 300 K) or methanol (below 300 K) as the temperature standard. Control could be maintained within $\pm$ 0.2 K. The spectrometer field is shimmed using the protons of the temperature standard. Running unlocked, the drift of the spectrometer is a negligible 0.001 ppm/day or less. Consequently, our system maintains experimentally a constant field over a 24 h time period at temperatures below 420 K. The spectrometer is run unlocked and the field is adjusted such that the methylene proton of an ethylene glycol sample has a resonance frequency of exactly 400.139 015 MHz at 300.0 K. Measurements at other temperatures are carried out at exactly the same field. The temperature-independent ^{129}Xe resonance frequency of an isolated Xe atom (the reference frequency for the ^{129}Xe chemical shifts reported here) should remain unchanged. We cannot check this directly with pure xenon gas sample which has a nonnegligible temperature dependence of its resonance frequency due to collision effects. However, we can use the next best system—the ^{13}C nucleus in methane gas has a known very small temperature dependence in its resonance frequency. Therefore we have used the ^{13}C resonance frequency in a $^{13}CH_4$ gas sample to fix the magnetic field as we determine the ^{1}H resonance frequency of the CH_2 protons in our ethylene glycol standard as a function of temperature. At each temperature, after shimming the CH_2 signal, the magnetic field is adjusted so that the ^{13}C resonance frequency is 100.613 805 MHz exactly. Then the $^1H(CH_2)$ frequency is measured. These $^1H(CH_2)$ resonance frequencies form a straight line in the range 300–420 K. These proton frequencies in ethylene glycol are used to set the magnetic field back to the same constant value for all ^{129}Xe measurements reported here. $^1H(CH_3)$ in methanol were used below room temperature. The resonance frequency of ^{129}Xe in an isolated xenon atom under these conditions is then effectively temperature independent (within $\pm$ 0.01 ppm over 100°).

Typical conditions are a transmitter frequency of 110.697 MHz, sweep width of 42.2 kHz, preacquisition delay of 60 μs, 1 K data points zero filled to 4 K, a relaxation delay of 10 s and 1000–10 000 scans. Since our sweep width is 42 kHz, it is necessary to consider the possibility of resonance offset effects; i.e., undesirable effects of nonuniformity in B_1 (effective) over our frequency range. We mapped out the effect by observing a xenon gas sample under systematic changes in B_0, while keeping the spectrometer conditions identical in our unlocked mode. We observed no change in signal intensity over the entire range. To obtain an adequate signal to noise (S/N) requires 2–24 h or more, depending on the sample and the desired S/N ratio. Although previous workers have used repetition rates of less than 1 s, our samples give no useful signals under these conditions. We attribute the difference to the presence of oxygen under the conditions used by previous workers.[39–41] It is well known from our gas phase studies that the spin relaxation times of ^{129}Xe in the gas phase are shortened drastically in the presence of oxygen due to the nuclear spin dipole–electron spin dipole mechanism.[42] T_1 for ^{129}Xe in zeolite Na*A* has been found recently to be 2.6 s.[43]

The collected free-induction decay (FID) is transformed, baseline corrected using a linear correction only, and transferred via FASTRAN (Farrar, University of Wisconsin) to a PC/AT clone, where line fitting is done with SPECTRA CALC (Galactic Industries Corp.) in order to obtain reliable peak frequencies and intensities. For the purpose of fitting, a line broadening of 300 Hz is used. This gives Fourier-transformed spectra which can be well represented by 500 points for nonlinear least-squares fitting. Our experience is that the peak center frequency can be obtained with an accuracy of $\pm$ 1–2% of full width at half-maximum (FWHM) or typically $\pm$ 0.1 ppm in our case. Peak intensities appear to be accurate to $\pm$ 3% for the more intense lines, with less certainty for weak lines. All ^{129}Xe chemical shifts reported here are positive (i.e., deshielded) relative to the isolated xenon atom.

III. RESULTS

The ^{129}Xe spectra obtained in one sample of xenon in zeolite Na*A* equilibrated at 500, 400, and 300 K are compared in Fig. 1. This is a high loading sample with a small amount of oxygen. For this figure only, all the spectra are taken at 300 K under conditions described in the Experimental section. At 300 K, the exchange rate for Xe atoms going from one cage to another is slow enough that the 500 and 400 K equilibrium distributions do not change perceptibly during the course of the several hours that it takes to collect the spectra. The individual peaks are unambiguously assignable, not just on the basis of this set of spectra, but on the basis of all other spectra we have taken on many samples of Xe in Na*A*. The peak at the low frequency end (right side of Fig. 1) is the signal for the free xenon gas in the sample. The pres-

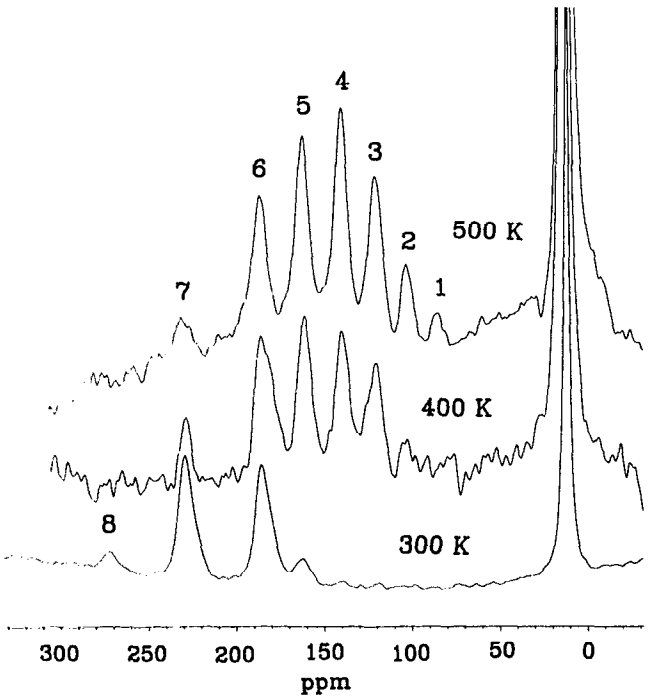

FIG. 1. ^{129}Xe NMR spectra of xenon in zeolite Na*A*, the same sample equilibrated at 300, 400, and 500 K. This particular sample included some oxygen. For this figure only, all spectra are taken at 300 K. The peaks on the right side of each spectrum corresponds to the free xenon gas. The peaks labeled 1, 2, 3,... are the signals of one Xe atom in an alpha cage, two Xe atoms in an alpha cage,... . The largest Xe_n cluster observed in this work is Xe_8.

ence of separate peaks for one Xe atom in a cavity, two Xe atoms in a cavity,..., up to eight Xe atoms in a cavity shows that, on the NMR time scale, the Xe_n clusters are isolated from each other at 300 K, i.e., the exchange rate at 300 K is much less than 2000/s. This is the first report of the ^{129}Xe signal from a cluster of eight xenon atoms.

A. The ^{129}Xe chemical shifts of the clusters

The Xe chemical shifts for the Xe_n clusters δ_n are independent of $\langle n \rangle$. The average values at 300 K are given in Table I. We also obtained spectra in samples doped with 1 amagat of oxygen gas in order to be able to compare our data with that of previous workers whose reported shifts were in samples exposed to air or deliberately doped with oxygen.[39–41] The comparison between our values for the Xe chemical shifts without oxygen (given in Table I), with oxygen, and from previous workers are shown in Fig. 2. The effect of oxygen is easily predictable from our previous work of ^{129}Xe chemical shifts in gaseous mixtures of xenon and oxygen.[44] Oxygen provides a collision-induced contact shift at the Xe nucleus in the transient Xe–O_2 molecule due to the nonvanishing average hyperfine interaction of the unpaired electrons with the ^{129}Xe nucleus. The contact shift is dependent on temperature, approaching a Curie-law dependence at low temperatures, and is dependent on the oxygen concentration. In Fig. 2, we note that the chemical shifts due to oxygen are in the direction expected (deshielding, i.e., to larger chemical shifts), largest for $n = 1$ and decreasing with n. It may be assumed that the O_2 molecules, being small enough to move freely in and out of the cavities, will be visiting cavities with different numbers of trapped Xe atoms. Xenon atoms in cavities with fewer Xe atoms, and hence larger "free volume," are expected to have, on the average, a higher exposure to O_2 molecules. As we see in Fig. 2, the chemical shifts for Xe_n clusters in samples with and without oxygen become closer together as n increases. Cavities with seven or eight Xe atoms see essentially no oxygen. It is therefore not surprising that we find δ_7 and δ_8 values (not shown in Fig. 2) to be the same in samples with or without oxygen. The differences between δ_n for $n = 1$–6 from previous work and from this work are consistent with contact shifts due to a statistical distribution of oxygen, although there may be other reasons for the differences. We have not shown the data of Samant *et al.*[41] on this plot; the lower S/N in the latter precludes a fair comparison.

One of the notable characteristics of the spectra typified by Fig. 1 is that the incremental chemical shifts between six and seven Xe atoms or seven and eight Xe atoms is nearly twice as large as that between the smaller clusters. Table I shows the average increments we have observed and are plotted in Fig. 3. For the smaller clusters, the incremental shift $(\delta_n - \delta_{n-1})$ at 300 K is about 20 ppm, reproducibly increasing from 17.5 to 25 ppm as n increases. The large step up to 44 ppm between Xe_6 and Xe_7 was also noted earlier.[39] The 44 ppm incremental shifts between six and seven, and between seven and eight Xe atoms are reproducible in all high loading samples of Na*A* that we have observed.

B. The temperature dependence of the ^{129}Xe chemical shift of each cluster

We have measured the temperature dependence of the spectra in low, medium, and high loading samples. The results are shown in Fig. 4. This is the first systematic temperature-dependent study of these shifts. There was some indica-

TABLE I. ^{129}Xe chemical shifts at 300 K in Xe_n clusters in zeolite Na*A* in ppm relative to a free Xe atom.

n	1	2	3	4	5	6	7	8
δ_n	74.8	92.3	111.7	133.2	158.4	183.5	228.3	272.3
$(\delta_n - \delta_{n-1})$		17.5	19.4	21.5	25.2	25.1	45.1	43.7
$(d\delta_n/dT)$	− 0.019	− 0.020	0	+ 0.020	+ 0.056	+ 0.095	+ 0.133	+ 0.125

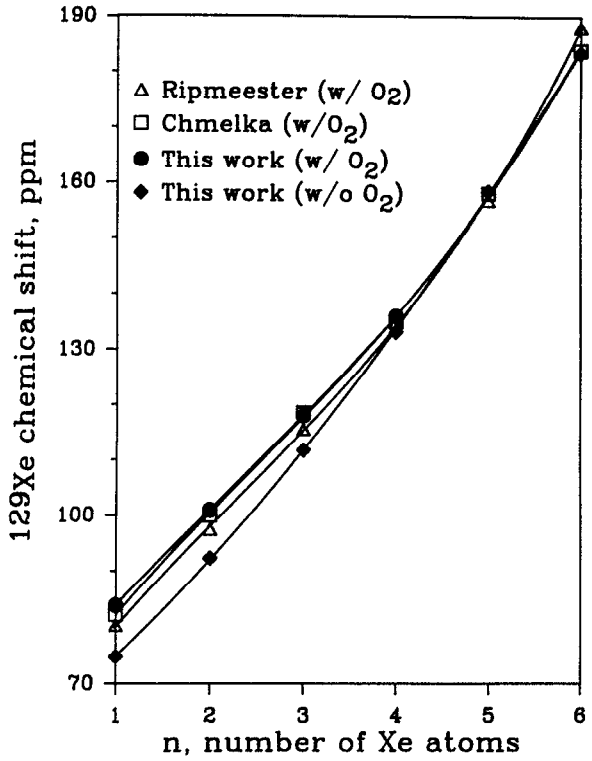

FIG. 2. ^{129}Xe NMR chemical shifts at 300 K corresponding to Xe, Xe_2, Xe_3, Xe_4, Xe_5, and Xe_6 clusters observed in this work in samples without oxygen or with 1 amagat of oxygen. Also shown, for comparison, are some values reported in the literature from the laboratories of Ripmeester (Ref. 28) (△) and Pines (Refs. 39 and 51) (□).

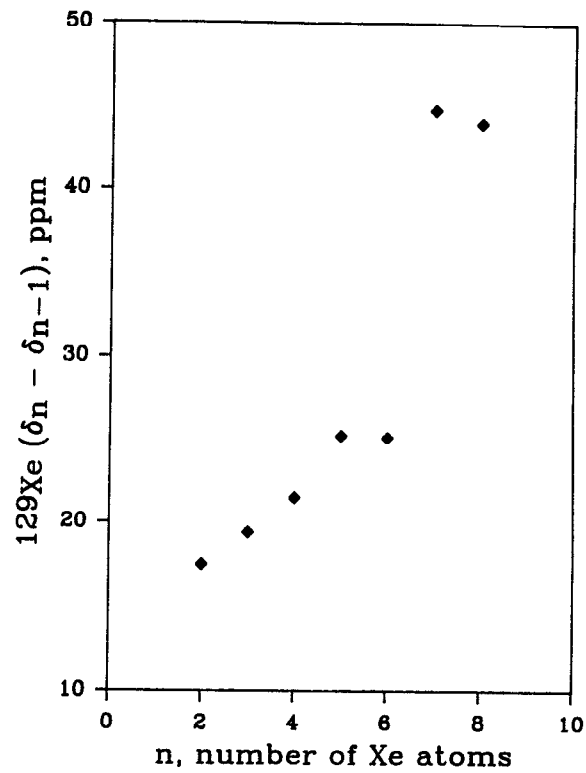

FIG. 3. The increments in the ^{129}Xe NMR chemical shifts at 300 K with increasing number of Xe atoms in the alpha cage.

tion by Ripmeester and Ratcliffe[40] that the spectra of Xe in zeolite Na*A* were relatively temperature independent. This is indeed the impression one would get on observing only the $n = 1$ to $n = 5$ peaks. What we find is that the temperature dependence of the Xe chemical shifts depends on the cluster size and is changing systematically in sign as one proceeds from the largest clusters to the smallest one. The chemical shift of Xe_3 has essentially no change with temperature. Xe_8 is not shown in this figure because this cluster disappears as the temperature is increased. We have, however, observed it below room temperature and its temperature dependence is also consistent with that of $n = 7$ in Fig. 4. The intrinsically interesting behavior is that of $n = 1$, a single Xe atom in a cavity. Here we observe a small, but definite increase of the chemical shift (more deshielding) with decreasing temperature. The slopes in Fig. 4 are recorded as $(d\delta_n/dT)$ in Table I.

C. The distribution of Xe atoms in the alpha cages

The intensities of the individual peaks can provide the relative fractions of the alpha cages containing Xe_n clusters, provided that the experimental conditions are such that the observed intensities are not T_1 limited. As mentioned in the Experimental section, we insure that we do not have a T_1 problem by taking spectra using a relaxation delay of 10 s. Nevertheless, spectra taken with a 5 s delay time are experi-

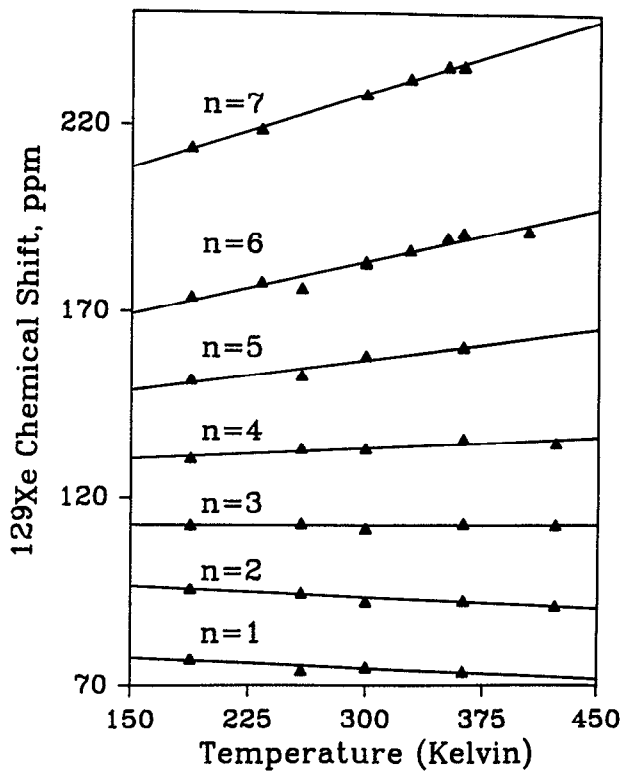

FIG. 4. The temperature dependence of the ^{129}Xe NMR chemical shift for each cluster Xe_n. The values of the slopes of the straight lines that are least-squares fits to the data are given in Table I.

mentally indistinguishable from those with a 10 s delay time. This would be expected if the spin–lattice relaxation time is about the same for all clusters.

The experimental distribution of occupancies of the alpha cages were obtained by fitting the spectra to Lorentzians. The areas A_n of the Lorentzians provide the fraction P_n of the alpha cages containing n Xe atoms

$$P_n = \langle n \rangle (A_n/n)/\Sigma_n A_n. \quad (2)$$

Here, $\langle n \rangle$ is the average number of Xe atoms per cage, obtained from a mass balance, as described in the Experimental section. The fraction of alpha cages which are empty are obtained by difference, since $\Sigma_n P_n = 1$. Where $P_0 = 0$, one can calculate a value of $\langle n \rangle$, which we call $\langle n \rangle_{\text{spect}}$, directly from the areas under the peaks

$$\langle n \rangle_{\text{spect}} = \Sigma_n A_n/\Sigma_n (A_n/n), \quad (3)$$

which should agree with $\langle n \rangle$ from the mass balance. This provides a check on our determination of $\langle n \rangle$ from mass balance. Where necessary to obtain a better fit, we use a combination of Lorentzians and Gaussians; the same proportion of Lorentzian/Gaussian for all peaks is employed in a given spectrum. The goal in the fitting is simply to obtain the areas in a quantitative manner. Table II shows the values of P_n we obtained for a low loading, medium loading, and a high loading sample at 300 K. For one of the medium loading samples, P_0 is very nearly zero. In this case, $\langle n \rangle = 5.44$ from mass balance agrees well with $\langle n \rangle = 5.79$, which is obtained directly from the spectrum. In the high loading sample, $\langle n \rangle = 7.03$ from mass balance differs by about 5% from $\langle n \rangle = 6.73$ directly from the spectrum, where $P_0 = 0$ can be assumed safely. Other examples are given in Tables II and III.

D. The approach to equilibrium

We have taken spectra of our samples as they approach equilibrium at 300 K over a period of months. The fitting and determination of $\langle n \rangle$ and P_n, more than just the visual qualitative changes in the spectrum, provide the means of determining when an equilibrium distribution of Xe atoms into the alpha cages has been reached. Since each crystallite of Na*A* is roughly 1 μ in size, or on the order of 1000 alpha cages across, most of the cages are empty at the outset and the occupancy numbers of the occupied cages near the outer surface are rather high. The distribution that is obtained at this stage is far from equilibrium; i.e., the $\langle n \rangle$ from the mass balance is in gross disagreement with that obtained directly from the spectrum because the fraction of empty cages is large. In this study, we have monitored the approach to equilibrium and, as described in the Experimental section, we used temperature programming to speed up the process. This is an important point which had been missed in some of the earlier work on NMR spectroscopy of molecules sorbed in zeolites. Depending on their sizes, molecules may take a long time to diffuse throughout the crystallites to achieve an equilibrium distribution and conclusions which may be based on spectra taken before equilibrium has been truly attained would be erroneous.

We have also taken the same samples to equilibrium at 360 K. The comparison is shown in Fig. 5 and the equilibrium distributions of Xe atoms in the alpha cages obtained at 360 K are given in Table III. The values of $\langle n \rangle$ are, of course, lower at 360 K compared to 300 K in the same sample.

IV. DISCUSSION

A. A model distribution in zeolite Na*A*, the hypergeometric distribution

The equilibrium distribution of N Xe atoms in m alpha cages depends on the temperature and the potential function that describes the intermolecular interactions between Xe and other Xe atoms, and the atoms constituting the alpha cage. The primary interactions are with the counterions Na^+ in the case of zeolite Na*A*, and the oxygens, since the Si and Al atoms of the zeolite framework are more remote from the Xe atom.

A model limiting case would be a strictly statistical distribution which takes the finite volumes of the Xe atoms into account. Guemez and Velasco have derived a distribution

TABLE II. The distribution of Xe atoms at various loadings at 300 K; P_n the fraction of alpha cages containing n atoms of xenon compared with H_n the hypergeometric distribution

	$\langle n \rangle = 1.46$		$\langle n \rangle = 3.21$		$\langle n \rangle = 5.44$		$\langle n \rangle = 7.03$	
	P_n	H_n	P_n	H_n	P_n	H_n	P_n	H_n
0	0.2419	0.1994	0.0283	0.0164	0	0.0001	0	0
1	0.3370	0.3562	0.1019	0.0881	0	0.0019	0	0
2	0.2311	0.2784	0.1817	0.2071	0	0.0139	0	0.0001
3	0.1171	0.1243	0.2468	0.2782	0.0236	0.0590	0	0.0010
4	0.0545	0.0347	0.2487	0.2337	0.0526	0.1569	0	0.0090
5	0.0184	0.0062	0.1418	0.1256	0.2376	0.2668	0.0278	0.0522
6	0	0.0007	0.0509	0.0422	0.4811	0.2835	0.3362	0.1893
7	0	0	0	0.0081	0.2050	0.1722	0.5175	0.3925
8	0	0	0	0.0007	0	0.0458	0.1185	0.3560
Δ^2	1.514	1.1916	2.072	1.924	0.822	1.740	0.491	0.847
$\langle n \rangle_{\text{spect}}$					5.79		6.727	

TABLE III. The distribution of Xe atoms at various loadings at 360 K; P_n the fraction of alpha cages containing n atoms of xenon compared with H_n the hypergeometric distribution

	$\langle n\rangle = 0.89$		$\langle n\rangle = 2.24$		$\langle n\rangle = 4.75$		$\langle n\rangle = 6.52$	
n	P_n	H_n	P_n	H_n	P_n	H_n	P_n	H_n
0	0.4193	0.3879	0.1551	0.0727	0	0.0007	0	0.0000
1	0.3483	0.3900	0.1459	0.2255	0	0.0086	0	0.0000
2	0.1625	0.1715	0.2424	0.3060	0.0201	0.0442	0	0.0008
3	0.0599	0.0431	0.2649	0.2373	0.1035	0.1294	0	0.0067
4	0.0100	0.0068	0.1482	0.1151	0.2766	0.2367	0.0579	0.0365
5	0	0.0007	0.0434	0.0357	0.3577	0.2772	0.1790	0.1282
6	0	0.0000	0	0.0069	0.2420	0.2029	0.4504	0.2814
7	0	0.0000	0	0.0008	0	0.0848	0.2874	0.3529
8	0	0.0000	0	0.0000	0	0.0155	0.0253	0.1936
Δ^2	0.900	0.792	1.960	1.610	1.023	1.929	0.797	1.207
$\langle n\rangle_{\text{spect}}$					4.70		6.04	

(hypergeometric distribution) that corresponds to this case by assuming that the molecules occupy mutually exclusive lattice sites in the subvolume (the alpha cage).[45] In the limit where the number of subvolumes and N are very large, it can be shown that their expression approaches the limiting form

$$H_n(\langle n\rangle) = \frac{\langle n\rangle^n (k - \langle n\rangle)^{(k-n)}}{k^k} \frac{k!}{n!(k-n)!}, \qquad (4)$$

where k is the maximum number of sites in an alpha cage, which we assume to be eight in the case of zeolite Na*A*. H_n designates the fraction of the alpha cages containing n Xe atoms according to the hypergeometric distribution. These fractions are shown in Fig. 6. The calculated H_n appropriate for the $\langle n\rangle$ of our experiments are given in Tables II and III

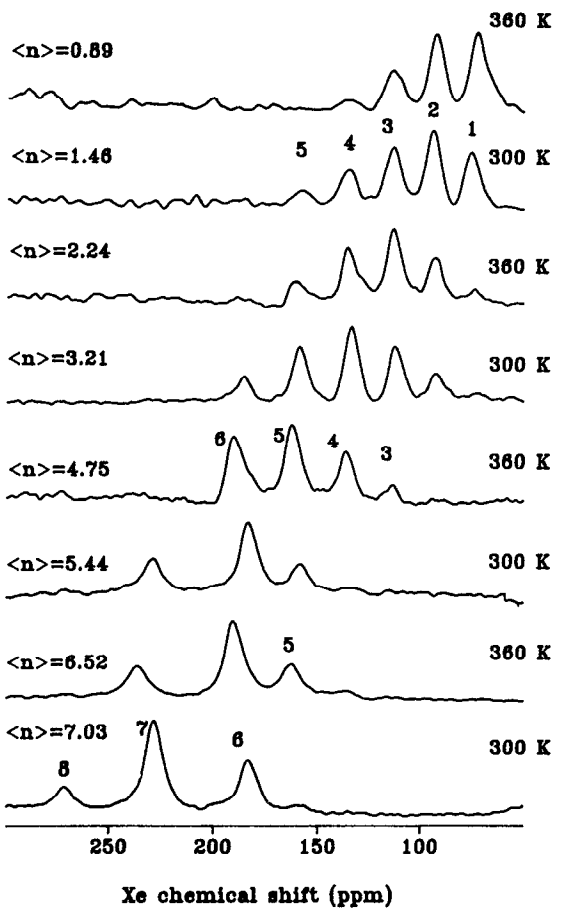

FIG. 5. ^{129}Xe NMR spectra of four samples. Each one was observed at equilibrium conditions at 300 and at 360 K. Thus, the equilibrium populations of Xe_n clusters at 300 and at 360 K are compared here.

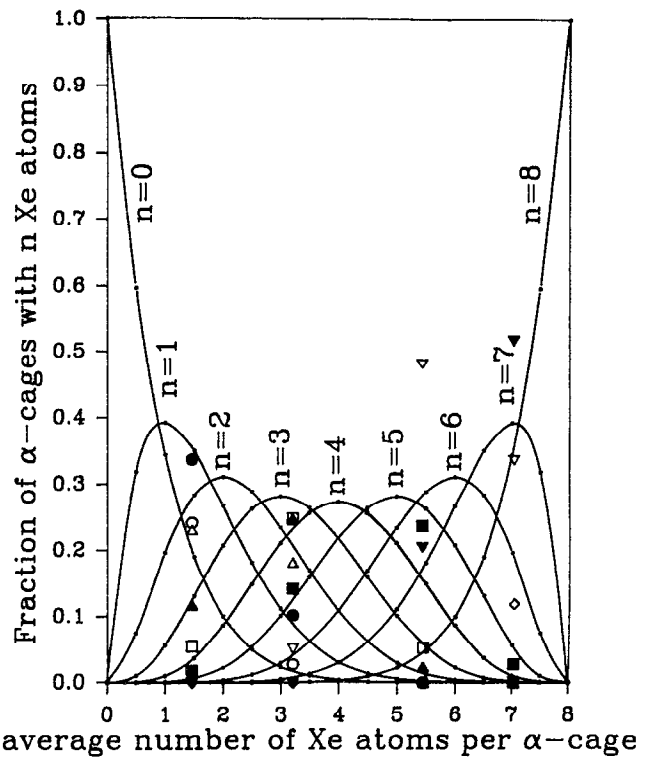

FIG. 6. The fraction H_n of alpha cages containing n Xe atoms, according to the hypergeometric distribution, as a function of xenon loading. The observed equilibrium distributions at 300 K are shown also. The symbols correspond to the following values of n: ○ = 0; ● = 1; △ = 2; ▲ = 3; □ = 4; ■ = 5; ▽ = 6; ▼ = 7; ◇ = 8.

for comparison with the experimental distributions. We have calculated spectra appropriate to the hypergeometric distribution model and show them in Figs. 7 and 8, in comparison with experiments at 300 and 360 K, respectively.

We find that the actual distributions at 300 and 360 K differ significantly from the hypergeometric distributions. No doubt, greater differences would be observed at lower temperatures than those of our experiments, but the equilibration time is so long at low temperatures that it is difficult to wait long enough for the steady state to be reached.

That the true distribution in zeolite Na*A* differs from the hypergeometric distribution implies that attractive Xe–Xe interactions do play a role. At low loading, we observe that high occupancies are more favored than the strictly statistical distribution. Because of the Xe–Xe attractive potential, clustering is favored, favoring high occupancies over lower ones, in comparison to hard spheres. Thus, the dispersion Δ^2 of the distribution given by

$$\Delta^2 \equiv (\langle n^2 \rangle - \langle n \rangle^2) = \Sigma_n n^2 P_n - (\Sigma_n n P_n)^2 \qquad (5)$$

is greater than that of the hypergeometric distribution at low loading. For example, for $\langle n \rangle = 1.46$, the experimental dispersion at 300 K $\Delta^2 = 1.514$ can be compared with 1.192 for the hypergeometric distribution. These dispersions are shown in Tables II and III.

At the medium loading, we find that the experimental distribution at 300 K is close to hypergeometric, although very slightly more peaked, compared to the hypergeometric distribution. At the highest loadings, we observe that the highest occupancies are significantly less favored than in the hypergeometric distribution. The experimental distribution is more peaked than the hypergeometric distribution at high $\langle n \rangle$; the dispersions are $\Delta^2_{\text{expt}} = 0.491$ compared to $\Delta^2_{\text{hyp}} = 0.847$ for $\langle n \rangle = 7.03$. This is in qualitative agreement with the results obtained by using a sphericalized version of a potential that had been derived for Xe atoms in faujasite to which had been added Lennard-Jones potentials for Xe–Xe interactions.[46] The simulations with this potential gave more peaked distributions than the hypergeometric distributions for the same size cavity. The potential functions that have been derived for Xe in zeolites *X* or *Y* (not the Na*A* that we use here) show that the radial distance from the center of the cavity corresponding to minimum energy is close to the wall.[33] Although the number of minimum energy sites and their locations depend on the molecule and the zeolite structure, except where the van der Waals radius of the guest molecule is nearly the same as the average radius of the cavity,[47] model potentials and simulations provide this general picture.[10,13,33,34,36,47] From these works, we can surmise that the low-energy arrangements of Xe_n in Na*A* are those in which the Xe atoms stay close to the wall of the cavity. As the minimum energy sites next to the wall become occupied, an easy fit of as many as six Xe atoms can be surmised from the known structure of Na*A*. The clusters of seven and eight would be less favored because the seventh and eighth Xe atoms find themselves in less energetically favorable locations in the cage and the Xe–Xe short-range repulsive interactions become important as the cage is overcrowded.

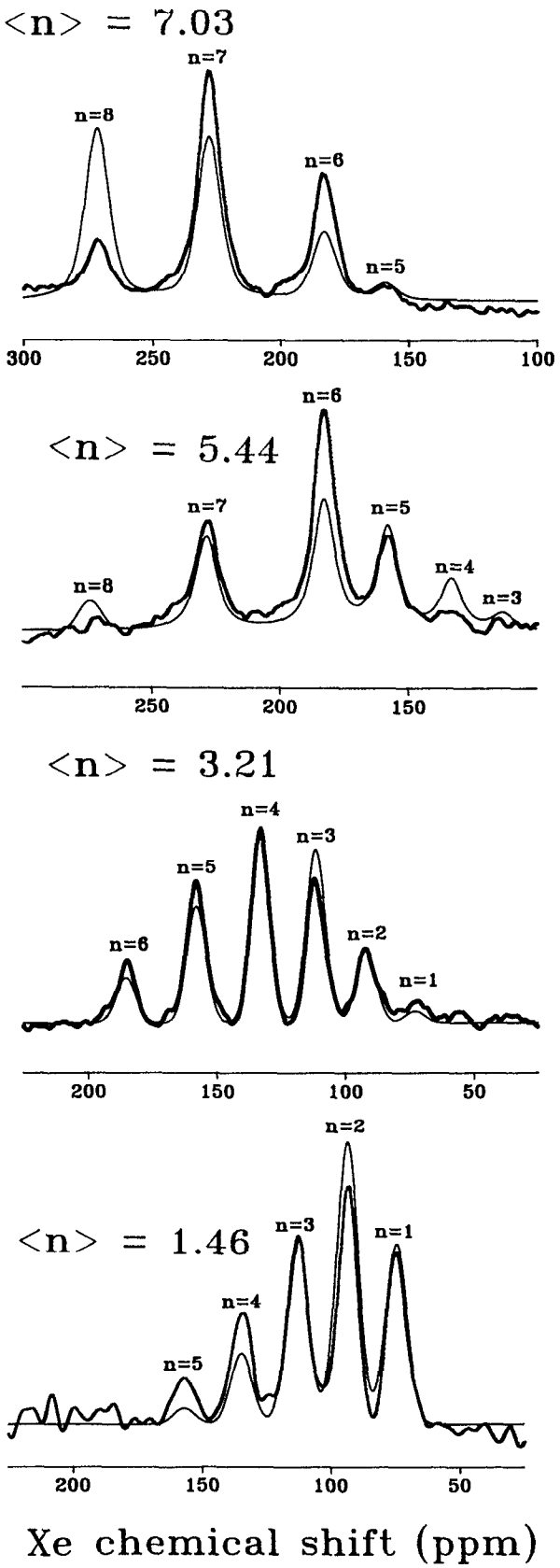

FIG. 7. Comparisons of the experimental ^{129}Xe NMR spectra at 300 K in four samples of xenon in zeolite Na*A* with the spectra predicted from the hypergeometric distribution. For example, the spectrum of a sample in which $\langle n \rangle = 1.46$ Xe atoms/cavity is compared with a calculated spectrum based on the hypergeometric distribution of occupancies for $\langle n \rangle = 1.46$. The total areas are made equal to correspond to an equal total number of xenon atoms.

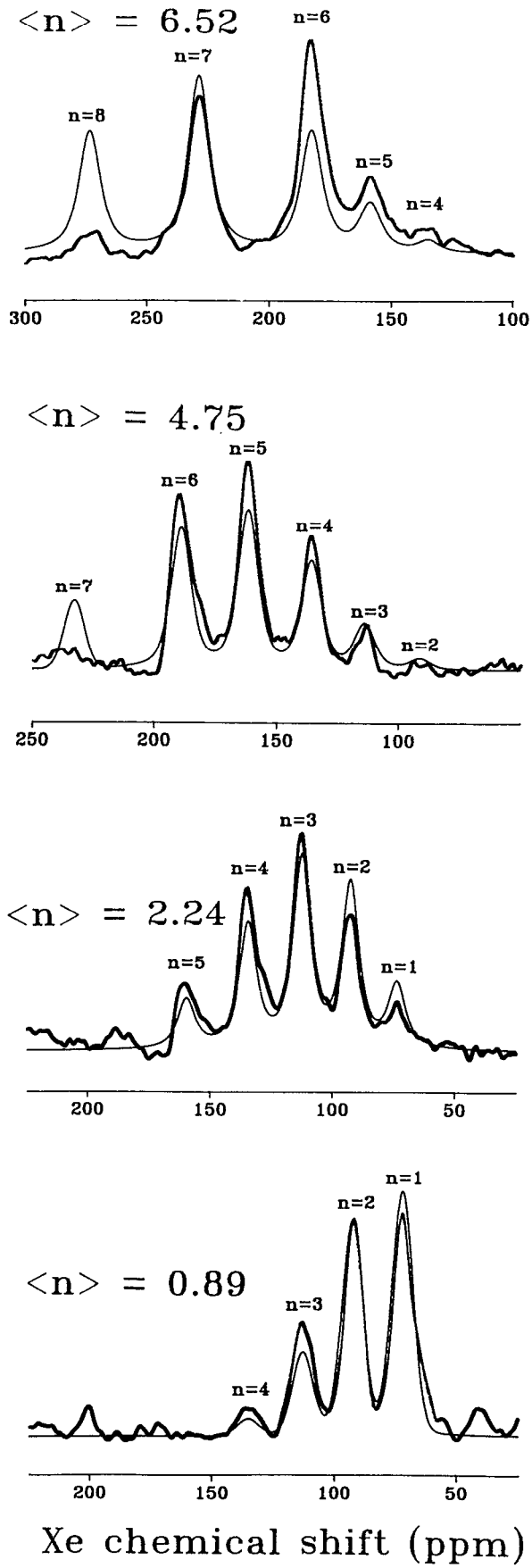

FIG. 8. The same as Fig. 7 except that the experimental spectra are for the equilibrium xenon distributions at 360 K.

B. The continuum model

Another model, called a continuum model, has been proposed by Rowlinson and Woods for the distribution of hard spheres in cavities, where the molecules are not restricted to specific lattice sites.[46] If each cage can hold up to eight Xe atoms, then we ask, what is the probability that there are n Xe atoms in the first cage, however, the $(N-n)$ other Xe atoms are distributed in the remaining cages? This calculation can be carried out numerically for any number of alpha cages using the formulas they have derived, but while it is done easily for only eight interconnected alpha cages in a unit cell of the zeolite, the results are not obviously generalizable to an analytic form in the limit of a very large number of Xe atoms and alpha cages. Nevertheless, for eight interconnected cages, we calculated these probabilities C_n which we compare with the hypergeometric probabilities H_n and with our experimental distribution P_n in Fig. 9.

As Rowlinson and Woods have found, continuum model distributions are more peaked (have smaller dispersion Δ^2) than the hypergeometric H_n. When compared with experiment, we note that the continuum model gives a distribution that is too peaked for all $\langle n \rangle$. It is closest to experiment for $\langle n \rangle$ around 5.0 and is much worse for low and high loading. The $n = 8$ peak is lower in experiment than predicted by any model. Although Rowlinson and Woods' earlier conclusion was that the continuum model is closer to the results of the molecular dynamics simulations using realistic potentials, we find that it does well only for $\langle n \rangle$ about 5.0, being significantly worse than the hypergeometric distribution at low loading and at high loading. It should be noted that this continuum calculation may not be statistically valid, since only eight alpha cages were considered.

We note in Fig. 9 that for $\langle n \rangle = 2.24$, we show a value of P_0 slightly greater than expected. This is a direct measure of the accumulated errors of our determination of $\langle n \rangle$ from mass balance and in the relative intensities of the observed peaks. Since $n = 0$ is not observed in the NMR spectrum, the combination of all these errors manifests itself as an error in the P_0 which is obtained by difference.

At low temperatures, attractive interactions between atoms favor the larger clusters. With increasing temperature, the distribution of Xe atoms into the alpha cages should become more nearly statistical; indeed the high temperature limit should be a statistical distribution of hard spheres. Comparing the distributions at 300 K with those at 360 K in Fig. 9, we note that the comparison between the statistical distributions and the experimental one is slightly more favorable for 360 than for 300 K (with one exception—$\langle n \rangle = 2.24$, where as mentioned above, we know P_0 is too large, but we did not attempt to renormalize the distribution). The equilibrium distributions at 523 K obtained by Chmelka *et al.*[39] were very close to the hypergeometric distribution appropriate for a maximum occupancy of seven Xe atoms for $\langle n \rangle = 1.5$, 2.9, and 4.9. The only discrepancy they observed was for $n = 5$, 6, and 7 in the sample with $\langle n \rangle = 5.8$.

Another distribution that has been considered, but which we do not include here, is the binomial distribution,

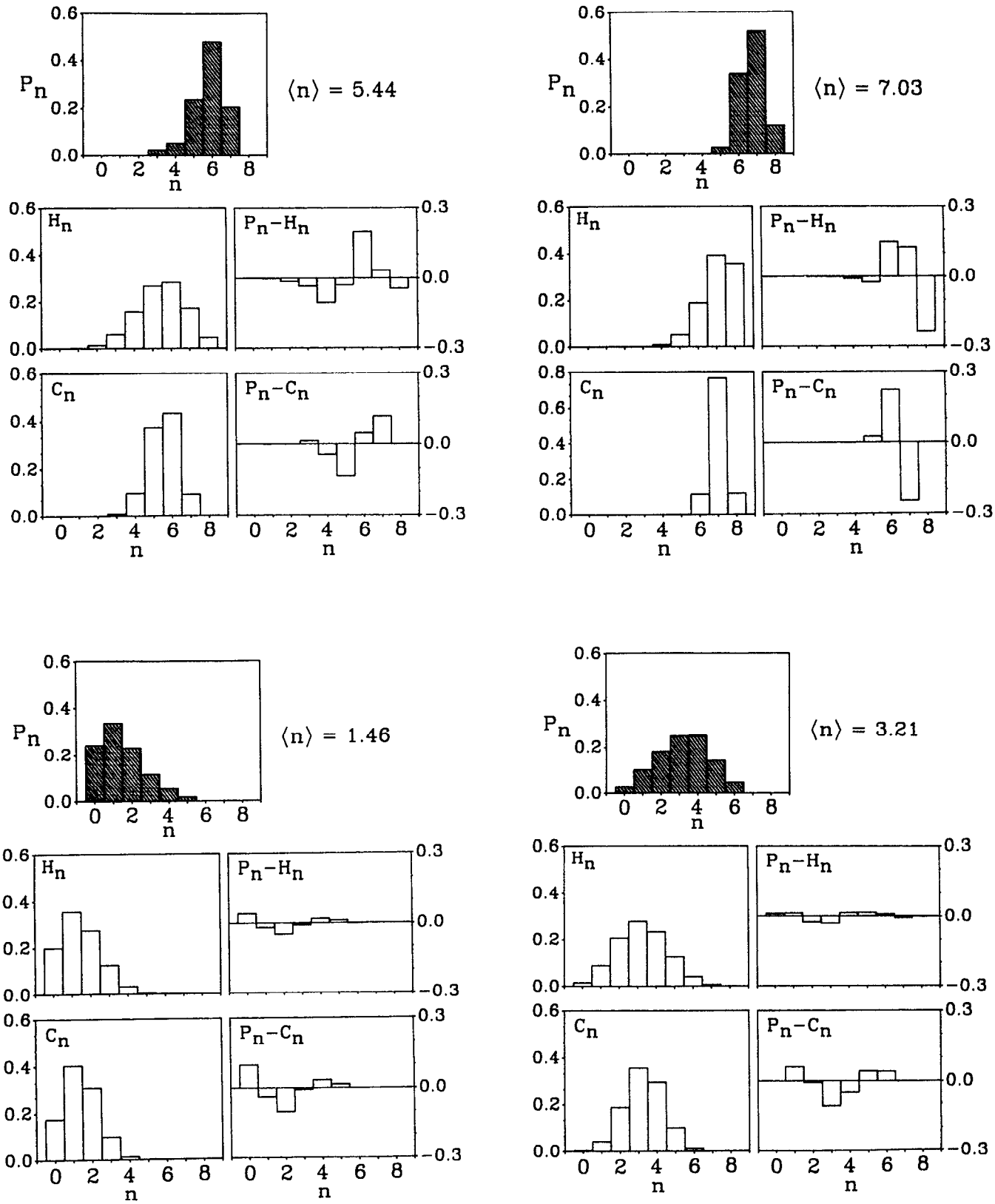

FIG. 9. The distribution of occupancies (fraction of alpha cages containing n Xe atoms is C_n) according to the continuum model of Rowlinson and Woods (Ref. 46) are compared with the hypergeometric distribution (H_n) and the experimental distribution (P_n) observed in samples of xenon in zeolite Na*A* under low, medium, and high loading at (a) 300 and (b) 360 K. In these figures, the value of $\langle n \rangle$ used in the calculation of C_n is that which is the closest value of $\langle n \rangle$ consistent with an integral number of Xe atoms in eight alpha cages, i.e., (a) $\langle n \rangle = 7.0$, 5.50, 3.25, and 1.50 and (b) 6.50, 4.75, 2.25, and 0.875, all of which are very close to the experimental values of $\langle n \rangle$.

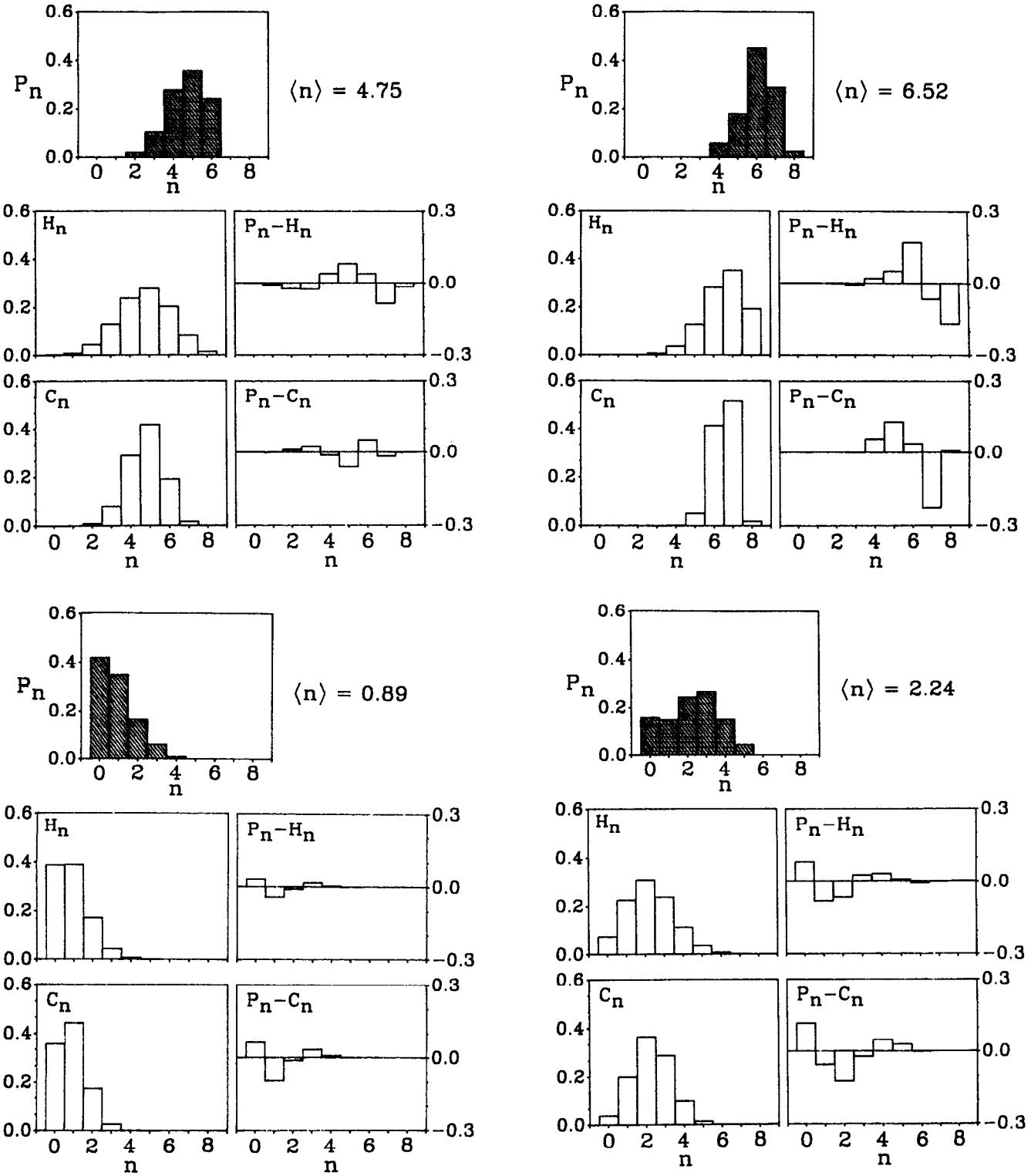

FIG. 9. (*Continued.*)

which has no provision for mutual exclusion. It could not apply to space-filling Xe atoms.

C. The ^{129}Xe chemical shifts in Na*A*

The Xe chemical shift $\delta_n(T)$ in the Xe_n clusters in this work are found (a) to be independent of $\langle n \rangle$; (b) to exhibit nearly equal increments for $n = 1$ to 6; and (c) to be dependent on temperature. That $\delta_n(T)$ appears to be invariant with respect to $\langle n \rangle$ seems to indicate that the influence of the neighboring clusters (in adjacent cages) on the chemical shift of ^{129}Xe in a given cluster is relatively small.

For up to six Xe atoms, the near additivity in chemical shift increments suggests that a sum of pairwise contribu-

tions to the shift is a good first approximation in the averaging of ^{129}Xe shielding over the configuration space of the Xe_n cluster. The nearly equal increments in the chemical shift in going from $n = 1$ to $n = 6$ are reminiscent of the $\sigma_1\rho$ term in the dilute gas, which increases the chemical shift with increasing density of the gas. However, the "effective" density coefficient of the chemical shift $(\delta_n - \delta_1)/(n/V)$ for Xe in an alpha cage of volume V is not equal to σ_1 obtained in the dilute gas limit. This is not surprising. In the very dilute xenon gas,[16] σ_1 is given by

$$\sigma_1(T) = \int_0^\infty 4\pi R^2 dR\, e^{-V(R)/kT}[\sigma(R) - \sigma(\infty)]. \quad (6)$$

σ_1 in the dilute gas has no "wall" effects. In the case of Xe in Na*A* zeolite, the Xe–Xe interaction occurs primarily between Xe atoms "*in contact*" with the cage walls, constituting a many-body interaction responsible for the observed shielding. This is much more complex than the binary collision model which can be used for dilute gases. Furthermore, the regions $R = r_{cage}$ to ∞ of the Xe_2 shielding surface are not included in the average chemical shift for the Xe_2 cluster in Na*A*, whereas they contribute significantly to σ_1 in the low density xenon gas. Thus, it is not surprising that the value of the "effective σ_1" that Fraissard obtained for $\langle n\rangle = 2.5$ in zeolite Ca*A*[48] was not equal to the σ_1 reported by us for pure xenon gas.[16]

The observed chemical shifts δ_n of ^{129}Xe in zeolite Na*A* are averages over the various configurations of a given Xe_n cluster in the presence of the additional potential due to the atoms of the cavity. For each configuration of a given Xe_n cluster, there is a corresponding ^{129}Xe nuclear magnetic shielding tensor for each magnetically inequivalent nuclear site in the cluster. The shieldings associated with each of these configurations are weighted by a factor $\exp(-V/kT)$ to obtain the thermal average shielding. The difference between the thermal average and the shielding of a free Xe atom is the chemical shift δ_n:

$$\delta_n = \sigma(\text{free Xe atom}) - \frac{\int d\mathbf{x}\,\sigma(\mathbf{x})\exp[-V(\mathbf{x})/kT]}{\int d\mathbf{x}\exp[-V(\mathbf{x})/kT]}, \quad (7)$$

where $\mathbf{x}$ is a point in configuration space. For these discussions, we need to have the nuclear magnetic shielding surfaces for the various xenon clusters.

Shielding calculations on Xe_2, Xe_3, etc. clusters are prohibitive. For the purpose of a qualitative interpretation of the experimental results, we consider the ^{39}Ar nuclear shielding as a model for the ^{129}Xe nuclear shielding. For ^{39}Ar, we have preliminary results on the *ab initio* calculations of the intermolecular contributions to shielding [at the coupled Hartree–Fock (CHF) level] in clusters such as Ar_2 and Ar_3 compared to an isolated Ar atom as a function of Ar–Ar distance. We have also calculated the ^{39}Ar shielding in the Ar atom in the presence of Na^+ ion. These *ab initio* calculations do not include second-order correlation effects.[49] Our hope is that the Ar clusters can be used to model the Xe_n clusters qualitatively. For the purpose of this discussion, we show only the intermolecular contributions to the Ar_2 and the $Ar\cdots Na^+$ shielding surfaces at the CHF level, calculated using the LORG (localized orbital local origin) method[50] in Fig. 10. Details on these calculations are to appear later.[49]

The ^{39}Ar model for the ^{129}Xe chemical shift demonstrates that the intermolecular contributions to the Ar deshielding can become very large at internuclear distances inside r_0 (the internuclear separation corresponding to $V = 0$). The changes are greater in the Ar_2 system than in the $Ar\cdots Na^+$ system. Figure 10 suggests that the intermolecular shielding function has a shape which is somewhat similar to that of the intermolecular potential energy function, but with a displaced minimum. The magnitudes of the changes in shielding at the same internuclear separation are much larger for the $Ar\cdots Ar$ than for the $Ar\cdots Na^+$ pair. In the averaging over the various configurations of a given Xe_n cluster, the ^{39}Ar model[49] suggests a marked deshielding due to the intermolecular interactions at distances shorter than the r_0 of the Ar–Ar potential function. For n Xe atoms in an alpha cage of volume V, the averaging occurs entirely over those values of $R_{Xe\text{-}Xe}$ that correspond to the various geometric configurations assumed by the cluster of n atoms, constrained to be between 0 and some value r_{max}, by the alpha cage. This restricted motional averaging process samples only the deshielded regions of the shielding surface for the Xe_n cluster, leading to positive chemical shifts.

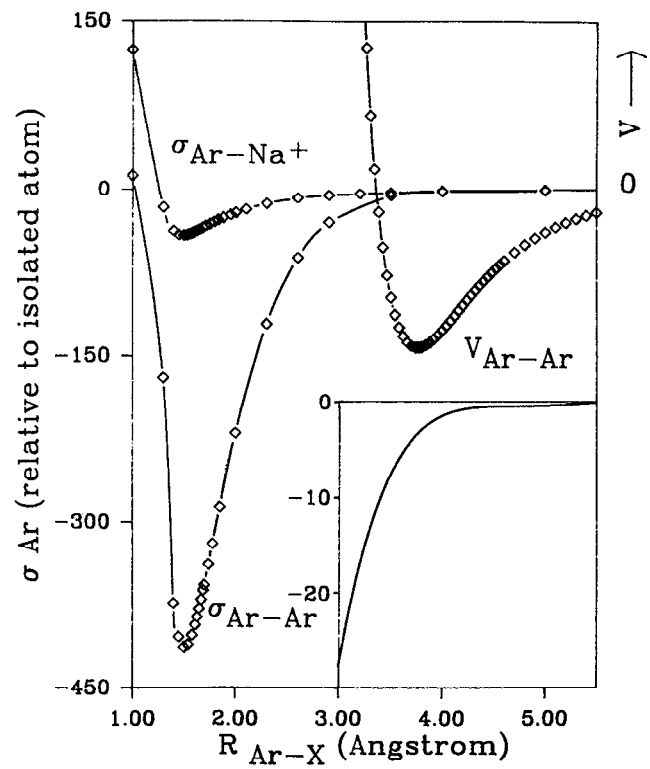

FIG. 10. The intermolecular contributions to the ^{39}Ar nuclear magnetic shielding surfaces for the Ar–Ar and the Ar–Na^+ systems obtained by *ab initio* calculations (LORG method) at the coupled Hartree–Fock level. (The ^{39}Ar chemical shifts relative to the isolated Ar atom are given by the same numbers as the values on the ordinate, but with opposite sign.) The intermolecular potential energy function for Ar–Ar is also shown (Ref. 53). The inset is an expanded version of the σ function for Ar–Ar.

That the incremental shift $(\delta_n - \delta_{n-1})$ increases slightly with n in Fig. 3, rather than remaining constant, can be interpreted as follows: the configurations of clusters of larger n, restricted by the confining alpha cage, involve shorter Xe–Xe distances than the configurations of clusters of smaller n. A greater sampling of the shorter distances give a more deshielded average.

In the plot of $(\delta_n - \delta_{n-1})$ vs n (shown in Fig. 3), the big jump in the increment $(\delta_n - \delta_{n-1})$ seems to indicate that the comfortable occupancy number for Xe atoms in zeolite Na*A* is 6. The chemical shifts δ_7 and δ_8 seen in Na*A* are much larger than expected because of the overcrowding possible in Na*A*, where Na^+ ions at site II locations block the windows that interconnect the cages.[31] The larger increments in the chemical shift of the Xe_7 and Xe_8 clusters are consistent with the much greater deshielding at $R_{Xe\text{-}Xe} < r_0$, averaged over the much narrower range of $R_{Xe\text{-}Xe}$ values possible in these clusters, when compared to the clusters Xe_n $(n = 2\text{–}6)$, in which $R_{Xe\text{-}Xe}$ is averaged primarily over the range $r_0 \leqslant R_{Xe\text{-}Xe} \leqslant r_{max}$. Here, r_{max} is the largest separation between two adjacent Xe hard spheres inside the alpha cage when the alpha cage is filled with seven or eight xenon atoms. It is tempting to attribute the large chemical shift in going from Xe_6 to Xe_7 to the more restricted set of $R_{Xe\text{-}Xe}$ values corresponding to the configuration space of the Xe_7 cluster, which are in the repulsive region of the cluster potential energy surface, similarly for the large chemical shift in going from Xe_7 to Xe_8.

D. The temperature dependence of δ_n in Na*A*

At each temperature, there will be an average ^{129}Xe chemical shift value δ_n, as discussed above, for the Xe_n cluster. How does the average value change with temperature? A change in temperature involves a change in the weighting factor $\exp(-V/kT)$ associated with the ^{129}Xe shielding corresponding to each configuration in Eq. (7). The factor $\exp(-V/kT)$ increases with increasing T if $R_{Xe\text{-}Xe}$ values are restricted to those for which $V > 0$. On the other hand, the factor $\exp(-V/kT)$ decreases with increasing T if $R_{Xe\text{-}Xe}$ are restricted to those values for which $V < 0$. A plausible explanation for the changing slopes in Fig. 4 is that the relative contributions of these two regions of configuration space change in going from low n to high n. Because of confinement, averaging the cluster configurations of Xe_2 or Xe_3 weights the longer Xe–Xe distances (corresponding to smaller chemical shifts) more with increasing temperature. On the other hand, with increasing temperature, the Xe_7 or Xe_8 cluster configurations weights the repulsive region (shorter Xe–Xe distances corresponding to larger chemical shifts) somewhat more.

The temperature dependence of the chemical shift of the single Xe atom in the Na*A* alpha cage is what one might expect if the ^{129}Xe nuclear shielding $\sigma(\mathbf{R})$ of the physisorbed xenon atom in the alpha cage is related to the potential energy $V(\mathbf{R})$. In the observed average chemical shift, various parts of the shielding surface are weighted by the factor $\exp[-V(\mathbf{R})/kT]$. At the lower temperatures, weighting most heavily those regions of $\mathbf{R}$ in which the Xe nucleus is most deshielded, produces a larger chemical shift with decreasing temperature. This is what we observe for δ_1.

Molecular dynamics simulations of one CH_4 molecule trapped inside a Na*A* cavity[10] indicate that one special lowest energy site exists, close to the unique Na^+ ion in the cage. If this were the case for Xe in Na*A*, we would have expected a different behavior than we found here. In particular, a special site would be expected to have a unique chemical shift which at low enough temperatures, would be the chemical shift for $n = 1$. Furthermore, the incremental shift in going from $n = 1$ to 2 would be expected to be considerably different from the others and the temperature dependence of $n = 1$ would be expected to be more pronounced and different from the others. We do not see that in Fig. 4.

V. CONCLUSIONS

We have observed Xe atoms trapped in the alpha cages of zeolite Na*A*. Singles (one Xe atom in a cavity) and clusters of 2 up to eight Xe atoms are individually observed in the ^{129}Xe spectrum. The temperature dependence of the ^{129}Xe chemical shift of each cluster has been measured in the range 188–421 K. We report for the first time the equilibrium distribution of occupancies of Xe atoms in the alpha cages at 300 and at 360 K for low, medium, and high xenon loading. It is found that the experimental distributions differ from the strictly statistical distributions of hard sphere atoms in mutually exclusive specific lattice sites (hypergeometric distribution), or the statistical distribution of freely moving hard spheres in alpha cages with no specific sites (continuum model). The experimental deviations from these statistical models can be explained by the attractive Xe–Xe interactions which favor clustering at medium loading and the higher energy associated with the overcrowded cage, disfavoring clusters of eight Xe atoms at high loadings.

The observed ^{129}Xe chemical shifts of individual clusters and their temperature dependences are interpreted by using the results of *ab initio* calculations of the intermolecular shielding function in the ^{39}Ar system as a model for the ^{129}Xe system. This model indicates that the chemical shifts due to the interaction of the Xe atom with the cations of the cage are not nearly as large as the chemical shifts due to the Xe–Xe interactions. The average chemical shifts observed for the clusters and their temperature dependences are interpreted in terms of the averaging of the ^{129}Xe shielding over various cluster configurations constrained by the alpha cage, weighted by a $\exp(-V/kT)$ factor corresponding to each configuration. The true Xe–Xe intermolecular shielding function is not yet available from *ab initio* calculations. However, this system is a good candidate for the density functional method developed by Grayce and Harris.[52] In principle, the density functional method could be used to calculate the intermolecular shielding function for any of the Xe_n clusters with an expected scaleup of computational effort that is not as steep as for conventional *ab initio* methods.

We are able to provide a physical interpretation of the

chemical shifts observed for Xe in the alpha cages of zeolite Na*A*, where trapping of the xenon atoms provides detailed information. In the general application of ^{129}Xe NMR spectroscopy to the characterization of zeolites and other microporous solids, only a single peak is observed, the result of fast exchange of Xe among multiple environments, in cavities containing different numbers of Xe atoms. In the following paper, the physical interpretation resulting from the measurements on Xe in zeolite Na*A* will be used to understand the results obtained in the ^{129}Xe NMR spectra of xenon in zeolite Ca*A*, where fast chemical exchange leads to a single featureless peak with a chemical shift dependent on xenon loading and temperature.

ACKNOWLEDGMENT

This research has been supported by the National Science Foundation (Grant No. CHE-8901426).

[1] See, e.g., *Studies in Surface Science and Catalysis*, edited by J. Klinowski and P. J. Barrie (Elsevier, Amsterdam, 1989), Vol. 52.
[2] P. Adams, J. R. Henderson, and J. P. R. B. Walton, J. Chem. Phys. **91**, 7173 (1989).
[3] T. K. Vanderlick, L. E. Scriven, and H. T. Davis, J. Chem. Phys. **90**, 2422 (1989).
[4] B. K. Peterson and K. E. Gubbins, Mol. Phys. **62**, 215 (1987).
[5] J. J. Magda, M. Tirrell, and H. T. Davis, J. Chem. Phys. **83**, 1888 (1985).
[6] J. P. Korb, M. Winterhalter, and H. M. McConnell, J. Chem. Phys. **80**, 1059 (1984).
[7] J. Tabony and J. P. Korb, Mol. Phys. **56**, 1281 (1985).
[8] M. Mackowiak, G. Liu, and J. Jonas, J. Chem. Phys. **93**, 2154 (1990); G. Liu, Y. Li, and J. Jonas, *ibid.* **95**, 6892 (1991).
[9] W. Heink, J. Kaerger, H. Pfeifer, and F. Stallmach, J. Am. Chem. Soc. **112**, 2175 (1990).
[10] E. Cohen de Lara, R. Kahn, and A. M. Goulay, J. Chem. Phys. **90**, 7482 (1990).
[11] S. Yashonath, P. Demontis, and M. L. Klein, J. Phys. Chem. **95**, 5881 (1991).
[12] S. Yashonath, P. Demontis, and M. L. Klein, Chem. Phys. Lett. **153**, 551 (1988).
[13] R. L. June, A. T. Bell, and D. N. Theodorou, J. Phys. Chem. **94**, 8232 (1990).
[14] S. Fritzsche, R. Haberlandt, J. Kaerger, H. Pfeifer, and M. Wolfsberg, Chem. Phys. Lett. **171**, 109 (1990).
[15] A. K. Jameson, C. J. Jameson, and H. S. Gutowsky, J. Chem. Phys. **53**, 2310 (1970).
[16] C. J. Jameson, A. K. Jameson, and S. M. Cohen, J. Chem. Phys. **62**, 4224 (1975).
[17] C. J. Jameson, Bull. Magn. Reson. **3**, 3 (1980).
[18] J. Jokisaari and P. Diehl, Liq. Cryst. **7**, 739 (1990).
[19] P. Diehl and J. Jokisaari, Chem. Phys. Lett. **165**, 389 (1990).
[20] J. Jokisaari, P. Diehl, and O. Muenster, Mol. Cryst. Liq. Cryst. **188**, 189 (1990).
[21] T. R. Stengle, N. V. Reo, and K. L. Williamson, J. Phys. Chem. **85**, 3772 (1981).
[22] T. R. Stengle, S. M. Hosseini, and K. L. Williamson, J. Solut. Chem. **15**, 777 (1986).
[23] J. Fraissard and T. Ito, Zeolites **8**, 350 (1988).
[24] J. Fraissard, Z. Phys. Chem. **152**, 159 (1987).
[25] E. G. Derouane and J. B. Nagy, Chem. Phys. Lett. **137**, 341 (1987).
[26] J. Demarquay and J. Fraissard, Chem. Phys. Lett. **136**, 314 (1987).
[27] D. W. Johnson and L. Griffiths, Zeolites **7**, 484 (1987).
[28] J. A. Ripmeester, C. I. Ratcliffe, and J. S. Tse, J. Chem. Soc., Faraday Trans. 1 **84**, 3731 (1988).
[29] B. F. Chmelka, J. G. Pearson, S. B. Liu, L. C. deMenorval, and A. Pines, J. Phys. Chem. **95**, 303 (1991).
[30] T. T. P. Cheung, J. Phys. Chem. **94**, 376 (1990).
[31] J. J. Pluth and J. V. Smith, J. Am. Chem. Soc. **102**, 4704 (1980).
[32] R. A. Aziz and M. J. Slaman, Mol. Phys. **57**, 825 (1986).
[33] G. B. Woods, A. Z. Panagiotopoulos, and J. S. Rowlinson, Mol. Phys. **63**, 49 (1988).
[34] G. B. Woods and J. S. Rowlinson, J. Chem. Soc. Faraday Trans 2 **85**, 765 (1989).
[35] S. Yashonath, Chem. Phys. Lett. **177**, 54 (1991).
[36] S. Yashonath, J. Phys. Chem. **95**, 5877 (1991).
[37] A. V. Kiselev and P. Q. Du, J. Chem. Soc., Faraday Trans. 2 **77**, 1 (1981).
[38] C. J. Jameson, A. K. Jameson, R. Gerald II, A. C. deDios, J. Chem. Phys. **96**, 1690 (1992).
[39] B. F. Chmelka, D. Raftery, A. V. McCormick, L. C. deMenorval, R. D. Levine, and A. Pines, Phys. Rev. Lett. **66**, 580 (1991); **67**, 931 (1991).
[40] J. A. Ripmeester and C. I. Ratcliffe, J. Phys. Chem. **94**, 7652 (1990).
[41] M. G. Samant, L. C. deMenorval, R. A. Dalla Betta, and M. Boudart, J. Phys. Chem. **92**, 3937 (1988).
[42] C. J. Jameson, A. K. Jameson, and J. K. Hwang, J. Chem. Phys. **89**, 4074 (1988).
[43] J. A. Ripmeester and C. I. Ratcliffe, Experimental NMR Conference, St. Louis, April 1991.
[44] C. J. Jameson, A. K. Jameson, and S. M. Cohen, Mol. Phys. **29**, 1919 (1975).
[45] J. Guemez and S. Velasco, Am. J. Phys. **55**, 154 (1987).
[46] J. S. Rowlinson and G. B. Woods, Physica A **164**, 117 (1990).
[47] I. Derycke, J. P. Vigneron, Ph. Lambin, A. A. Lucas, and E. G. Derouane, J. Chem. Phys. **94**, 4620 (1991).
[48] T. Ito and J. Fraissard, J. Chem. Phys. **76**, 5225 (1982).
[49] C. J. Jameson and A. C. de Dios (to be published).
[50] A. E. Hansen and T. D. Bouman, J. Chem. Phys. **82**, 5035 (1985).
[51] A. V. McCormick and B. F. Chmelka, Mol. Phys. **73**, 603 (1991).
[52] C. J. Grayce and R. A. Harris, Mol. Phys. **72**, 523 (1991).
[53] G. C. Maitland, M. Rigby, E. B. Smith, and W. A. Wakeham, *Intermolecular Forces, their Origin and Determination* (Clarendon, Oxford, 1981), Appendix 9.